Supported Natural Membranes on Microspheres for Protein–Protein Interaction Studies

Sudheer K. Cheppali, Raviv Dharan, Roni Katzenelson, and Raya Sorkin*

Cite This: https://doi.org/10.1021/acsami.2c13095
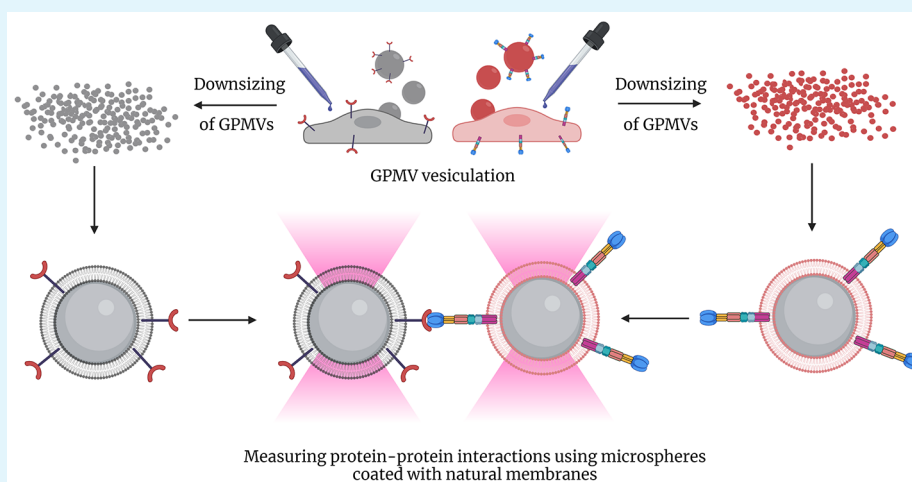
Read Online

| ACCESS | | Metrics & More | | Article Recommendations | | Supporting Information |

Measuring protein–protein interactions using microspheres coated with natural membranes

ABSTRACT: Multiple biological and pathological processes, such as signaling, cell–cell communication, and infection by various viruses, occur at the plasma membrane. The eukaryotic plasma membrane is made up of thousands of different lipids, membrane proteins, and glycolipids, and its composition is dynamic and constantly changing. Due to the central importance of membranes on the one hand and their complexity on the other, membrane model systems are instrumental for interrogating membrane-related biological processes. Here, we develop a new tool for protein–membrane interaction studies. Our method is based on natural membranes obtained from extracellular vesicles. We form membrane bilayers supported on polystyrene microspheres that can be trapped and manipulated using optical tweezers. This method allows working with membrane proteins of interest within a background of native membrane components where their correct orientation is preserved. We demonstrate our method's applicability by successfully measuring the interaction forces between the Spike protein of SARS-CoV-2 and its human receptor, ACE2. We further show that these interactions are blocked by the addition of an antibody against the receptor binding domain of the Spike protein. Our approach is versatile and broadly applicable for various membrane biology and biophysics questions.

KEYWORDS: supported membranes, optical tweezers, force spectroscopy, SARS-CoV-2, membrane biophysics

■ INTRODUCTION

The eukaryotic plasma membrane can be thought of as a two-dimensional solution of integral membrane proteins in a lipid bilayer solvent, where membrane proteins can constitute about 50% of the total membrane area.[1,2] Studying integral membrane proteins is highly important as they play ubiquitous roles in many physiological processes such as cell signaling, cell–cell communication, and host–pathogen interactions, among others.[3–5] These proteins require a membranous environment for their activity. A common method to study such proteins is to reconstitute them within synthetic liposomes.[6] Purification and reconstitution of proteins of interest in synthetic membranes can affect their stability, solubility, and activity,[7] while optimizing the reconstitution

conditions for every membrane protein is time-consuming and costly.[8–10]

Alternative model systems that can be used to study membrane proteins are natural membranes shed from the cellular plasma membrane: large vesicles termed Giant Plasma Membrane Vesicles (GPMVs)[11] and smaller vesicles termed blebs.[12–14] The shedding of such vesicles is induced by

ACS Publications

chemical treatments,[15,16] as opposed to extracellular vesicles such as exosomes that are naturally secreted by cells.[17] This allows obtaining membrane proteins in their correct orientation and natural membrane environment. In particular, both types of vesicles have been used to form supported plasma membrane bilayers (SPMBs) that are compatible with various experimental methods, such as TIRF[18,19] and AFM.[18,20] Blebs can be used together with synthetic liposomes to form supported bilayers for various applications, e.g., biosensors and screening of transmembrane protein modulators.[21,22] Several studies have shown that SPMB can be formed from GPMVs on a SiO$_2$ surface by exposing the surface layer to an air−water interface[23] or through acoustic radiation to induce the rupture of GPMVs.[24] Recently, Teiwes and colleagues have shown that SPMBs can be formed by spreading GPMVs on SiO$_2$ activated by oxygen plasma.[25] Out of all the methods outlined above, only the use of blebs in combination with synthetic liposomes led to continuous supported membrane bilayers formation,[19,22] while the rest resulted in the formation of large membrane patches.[23−25] All of these SPMBs were formed on a planar surface and mainly used to study protein dynamics and interactions.

An attractive approach for quantitative studies of protein−protein or protein−membrane interactions is by using optical tweezers.[26−33] Several experimental schemes have been used; one approach is using microscopic beads coated with synthetic membranes, where ectodomains of proteins of interest are tethered to the microspheres using linkers.[27,29] Another approach is using soluble ectodomains with membrane-coated beads,[26,34−36] or binding proteins to synthetic membranes via His-tag on the protein interacting with Ni-NTA headgroup-modified lipids.[36] All of these studies involved microspheres coated with synthetic membranes and truncated rather than full-length proteins. Coating natural membranes on a microsphere has not been performed so far.

In this work, we describe a new method to coat natural membranes containing proteins of interest on microspheres for measuring protein−protein interactions using optical tweezers. Although cell blebs are of suitable size for microsphere coating, their concentration is very low. Since the surface area of microspheres compared to a planar surface, for a typical experiment, is very large, more material is needed for the coating. To increase the yield of natural membranes obtained from cells, we used giant plasma membrane vesicles (GPMVs), which we downsized to obtain a large number of small vesicles optimal for deposition on microspheres.

To validate our method and the presence of functional and properly oriented proteins on the microspheres, we performed protein−protein interaction studies using human ACE2 and the Spike protein of the SARS-CoV-2. Our approach is versatile and broadly applicable for various membrane biology and biophysics questions.

■ METHODS

Plasmid Preparation and HEK293T Cell Transfection. HEK293T cells were cultivated in DMEM medium containing 10% FBS, 2 mM glutamate, 1 mM sodium pyruvate, 50 IU/mL penicillin, and 50 μg/mL streptomycin antibiotics (Thermo Fisher Scientific, USA) in T25 cell culture flasks at 37 °C and 5% CO$_2$. Cell dissociation was performed with 1 mL of Trypsin-EDTA (Fisher Scientific, U.K.). Cells were collected after centrifugation at 50g for 2.5 min, diluted 1:12, and plated in 25 cm^2 culture flasks coated with 0.1 μg/mL poly-L-lysine (Sigma) and cultured until the confluency reached 50−60% and no less than 24 h before transfection.

The SARS-CoV-2 Spike full-length gene (no. 43740568) containing a C-terminal flag-tag (Spike) was cloned into a pCAGGS vector, and the ACE2-GFP (ACE2) was purchased from Addgene (no. 154962). Plasmid scale-up was performed using Nucleobond midi-plasmid purification kit (Nucelobond no. 740410) using the manufacturer's protocol, and the sequence was confirmed using Sanger sequencing at the TAU sequencing unit. ~5 μg of either Spike or ACE2 plasmid was transiently transfected using a lipofectamine 2000 reagent (Invitrogen, no. 11668037) according to the manufacturer's protocol. Cells were grown in an incubator at 37 °C and 5% CO$_2$ for at least 24 h to obtain an optimal transfection yield.

Membrane Labeling and GPMV Production. HEK-293T cell plasma membranes were labeled using a lipophilic dye C12-DiI (DiI) (Thermo Fisher Scientific, USA). For labeling, culture medium was removed, and cells were gently washed with 4 mL of PBS, followed by addition of 2 μg/mL DiI in a buffer containing 20 mM HEPES, 150 mM NaCl, and 2 mM CaCl$_2$ at pH 7.4 (GPMV buffer), and incubated for 15−20 min at 37 °C. After incubation, cells were washed 3 times with a GPMV buffer to remove excess dye. To induce vesiculation of ACE2 transfected cells, the cells were incubated for >6 h at room temperature in 1 mL of active vesiculation buffer containing 2 mM dithiothreitol (DTT) and 27.6 mM formaldehyde in GPMV buffer.[37] In the case of GPMV production from Spike transfected cells, vesiculation was induced by the addition of DTT (Roche) + formaldehyde (Sigma) as described above.[38,39] The GPMVs were collected using a cut pipette tip and used immediately on the same day. An additional centrifugation step (100g for 2 min) was employed to remove any cell debris.

Downsizing of GPMVs and Formation of Supported Plasma Membrane Bilayers. GPMVs were downsized manually using a mini-extruder (Avanti polar lipids, USA). ~1 mL of the suspension containing GPMVs was very slowly passed through a 100 nm filter 33 times, and the final extruded suspension was collected for further experiments. Prior to SPMB deposition on glass slides, the surfaces were washed with Milli-Q water followed by sonication in ethanol for 3−4 min for 3 cycles, another wash with Milli-Q water, and then dried using airflow. SPMB were formed by spreading downsized GPMVs on a clean glass slide and incubating for 15−30 min at room temperature. The deposited vesicles underwent a gentle wash with GPMV buffer and were imaged with and without the addition of synthetic liposomes using an Olympus EP50 microscope with a 40× objective.

Liposome Preparation. Lipids purchased from Avanti polar lipids (Alabama, USA) were dissolved in chloroform (Sigma). DOPC, DOPS, and Cholesterol were used in a 5:2:3 molar ratio for unlabeled vesicles, and 0.5% of Rhodamine-PE was added to prepare fluorescent liposomes. The solvent was dried under a gentle stream of argon gas followed by vacuum desiccation for at least 4 h. The lipid film formed at the bottom of the glass tube was hydrated with 1 mL of GPMV buffer. Small unilamellar vesicles (SUVs) were produced by vortexing the lipids in buffer followed by sonication for 0.5−1 min and finally extrusion through a 100 nm polycarbonate filter using a mini extruder from Avanti Polar Lipids (Alabama, USA).

Fluorescence Recovery after Photobleaching. Fluorescence recovery after photobleaching (FRAP) of the SPMB was carried out using a Leica SP8 TCS HyD confocal microscope (Leica Microsystems, Germany). Bilayers were imaged with a 60× oil immersion lens using FRAP settings of λ_{ex} = 552 nm laser excitation wavelength and λ_{em} = 570−650 emission wavelength range. A circular region of interest (r = 10 μm) was bleached by a short laser pulse, and the fluorescence recovery was monitored against a reference region of interest (ROI) within the same membrane area. Images were analyzed using Fiji ImageJ, and the diffusion coefficients were calculated using the Soumpasis method.[40] A similar method was used to calculate the diffusion coefficient of bilayers containing synthetic lipids, DOPC/DOPS/Cholesterol/Rh-PE in a 49.5:20:30:0.5 molar ratio. For FRAP experiments on microspheres, exponential function fitting was used as the assumptions underlying the Soumpasis method are not valid in this case.

Size and Concentration Measurements. The size and concentration of downsized natural vesicles were measured by

nanoparticle tracking analysis (NTA) using the NanoSight NS3000 (Malvern Instruments, Worcestershire, U.K.). For each sample, at least 3−5 video recordings of 60 s were collected with a constant camera level and threshold for all samples. Measurements were performed at 25 °C. Analysis of the videos was performed using the software provided by the supplier. Concentration measurements after downsizing were routinely performed, in order to maintain the desired natural to synthetic vesicle ratio in the coating.

The hydrodynamic radius of the vesicles was also analyzed by dynamic light scattering using the Malvern nano ZS zeta sizer (Malvern Instruments, Worcestershire, U.K) in GPMV buffer.

Atomic Force Microscopy. Atomic force microscopy (AFM) imaging of downsized GPMVs and membrane bilayers was conducted using a JPK Nanowizard4 XP AFM from Bruker, USA. Imaging was performed with DNP-10 cantilevers ($k = 0.12$ N/m) using the quantitative imaging (QI) mode at room temperature in GPMV buffer. Images were analyzed using the JPK software.

Membrane Coating on Microspheres. Polystyrene micro-spheres (beads) of 3.15 μm diameter were obtained from Spherotech, Inc. (Lake Forest, USA). Before coating, microspheres were suspended in GPMV buffer and washed through 3 cycles of vortexing followed by centrifugation at 900 × g for 3 min. The microspheres were resuspended in ~500 μL of downsized GPMVs for coating and incubated overnight at slow rotation (15 rotations/min) using a cyclomixer. To obtain uniform coating of the membrane on the microspheres, liposomes were added in a 1:50 ratio of downsized GPMVs: liposomes. The coated microspheres were collected and washed again 3 times to remove any unbound material. In the case of GPMVs containing DiI, washing was thoroughly performed at least 5−6 times to remove any free DiI dye. Confocal fluorescence imaging of the DiI labeled microspheres was conducted using the confocal setup of the C-trap optical tweezers from LUMICKS. For fluorescence scans, microspheres were excited with a 561 nm wavelength laser, and emission was collected in the 580−630 nm range.

For protein−protein interactions, one set of washed microspheres was incubated with downsized GPMVs containing ACE2 and another with downsized GPMVs containing Spike and labeled with DiI. For antibody blocking, microspheres coated with downsized GPMVs containing Spike were separated into two groups. One set was used as-is for measuring ACE2−Spike interactions, while the other set of microspheres was incubated with anti-receptor binding domain (RBD) monoclonal antibody (Ab) for 1−2 h in a microcentrifuge tube, washed, and used immediately to measure the ACE2−Spike interactions in the optical tweezers setup.

Syncytium Assay. Plasmid coding for human ACE2 together with a GFP expression plasmid, and Spike plasmids, were transfected into two different HEK293T cell culture plates as described above. ACE2+GFP cotransfected cells were detached using pre-warmed PBS containing EDTA and added to the Spike transfected HEK293T cells. The cells were incubated for 2 h at 37 °C and 5% CO$_2$, followed by addition of 100 μg of trypsin and further incubation for 6−8 h. The syncytia formed were imaged using an Olympus EP50 microscope and an Olympus FV3000 confocal microscope. No trypsin was added to the control samples.

Confocal Microscopy. Confocal images of the cells and GPMVs and syncytium imaging were carried out using an Olympus FluoView FV 3000 confocal microscope under 20× magnification. Images were collected using cell vision software.

Optical Tweezers (OTs). The experiments were performed using a C-trap confocal fluorescence optical tweezers setup (LUMICKS) made of an inverted microscope based on a water-immersion objective (NA 1.2) together with a condenser top lens placed above the flow cell. The optical traps are generated by splitting a 10 W 1064 nm laser into two orthogonally polarized, independently steerable optical traps. To steer the two traps, one coarse-positioning piezo stepper mirror and one accurate piezo mirror were used. Optical traps were used to capture polystyrene microbeads. The displacement of the trapped beads from the center of the trap was measured and converted into a force signal by back-focal plane interferometry of the condenser lens using two position-sensitive detectors. The samples were illuminated by a bright field 850 nm LED and imaged in transmission onto a metal-oxide semiconductor (CMOS) camera. For the confocal fluorescence microscopy, the C-trap uses a 3-color, fiber-coupled laser with wavelengths of 488, 561, and 638 nm for fluorescence excitation. Scanning was performed using a fast tip/tilt piezo mirror. For confocal detection, the emitted fluorescence was descanned, separated from the excitation by a dichroic mirror, and filtered using emission filters (blue, 500−550 nm; green, 575−625 nm; red, 650−750 nm). Photons were counted using fiber-coupled single-photon counting modules. The multimode fibers serve as pinholes providing background rejection. For imaging membrane-coated microspheres, confocal scans were performed at a constant z position. The microspheres were excited with a $\lambda_{ex} = 561$ nm laser, and emission was collected in $\lambda_{em} = 575−625$ nm for DiI and $\lambda_{ex} = 488$ nm laser and $\lambda_{em} = 500−550$ for GFP. 10% laser power was used for all of the excitation measurements. 54.35 μW is the maximal laser power.

For ACE2−Spike interaction studies, two microsphere sets, one harboring ACE2 and another harboring Spike, were injected into different channels of a 5-channel flow cell (Lumicks, The Nether-lands) and captured in two optical traps.

Once trapped, the two microspheres were moved into another channel containing buffer, and the interactions were performed in an approach−retraction routine by keeping one bead constant and moving the other, as described previously.[26] The traps were calibrated using power spectral analysis and had a stiffness (k) of 0.38−0.405 pN/nm. All experiments were carried out at a constant z position and trapping power. Ten approach−retraction cycles per each pair of beads were performed, and the resulting rupture forces were measured as described previously.[26,35]

Protein Density Calculation. ACE2−-GFP density on GPMVs was determined as described earlier.[9,41] Briefly, fluorescence intensity of the GPMVs was quantified according to the blue channel photon count of the confocal image. In separate experiments, GUVs containing 0.1% Oregon green-DHPE (OG) were imaged to provide a reference signal of known fluorophore concentration in the membrane. All of the experiments were performed under the same settings. The fluorescence intensity of the fluorophore was related to the fluorophore density as

$$x_{GUV}^{OG} = Cp \times I_{GUV}^{OG}$$

where x is the mole fraction of the fluorophore in the GUV and Cp depends on the confocal setup parameters and fluorescence yield of the fluorophore and I is the fluorescence intensity of the fluorophore.

To compensate for the fluorescence yield difference between OG and GFP, the fluorescent intensities of water-solvated OG and GFP were measured.[42] The mole fraction of the protein in the GPMV was calculated as follows:

$$x_{GPMV}^{ACE2−GFP} = \frac{x_{GUV}^{OG}}{I_{GUV}^{OG}} \times \frac{I_{GPMV}^{ACE2−GFP}}{I_{Soluble}^{GFP}/I_{Soluble}^{OG}}$$

protein mole fraction on the microspheres was calculated from the fluorescence intensity as follows:

$$x_{microsphre}^{ACE2−GFP} = \frac{x_{microsphre}^{OG}}{I_{microsphre}^{OG}} \times \frac{I_{microsphere}^{ACE2−GFP}}{I_{Soluble}^{GFP}/I_{Soluble}^{OG}}$$

where $I_{microsphere}^{OG}$ is the intensity of the microspheres coated with liposomes containing known concentration of OG (Figure S6).

Data Analysis. All of the data from the optical tweezers experiments were collected using a commercial software from Lumicks called "Bluelake" and exported as h5 files. Analyses of the probability of interactions, rupture forces, and photon counts in regions of interest were carried out using custom-written Python scripts using the Python "pylake" package from Lumicks.

Statistical Analysis. NTA measurements of downsized GPMVs were performed for 3 independent samples. Mean values and their standard deviations (SDs) are reported. AFM imaging of the SPMB
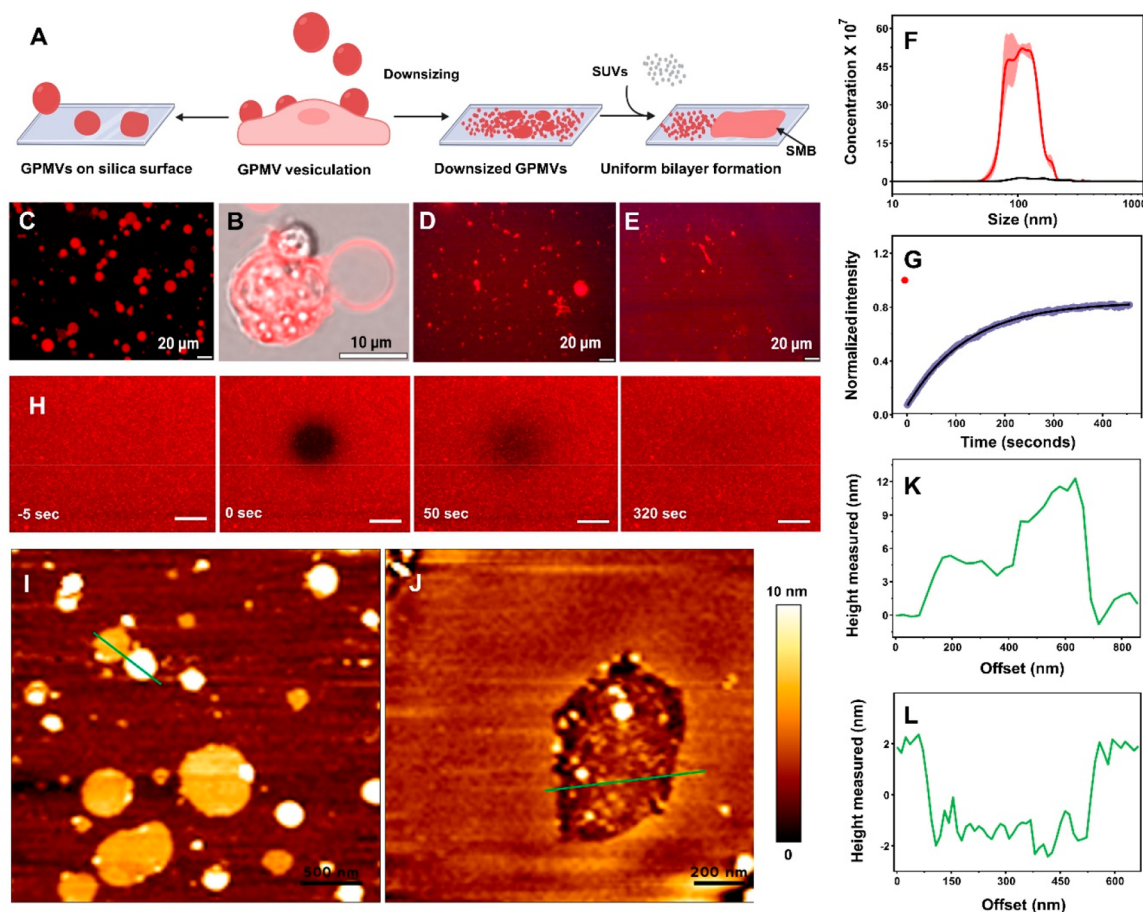
Figure 1. Formation and characterization of supported plasma membrane bilayers (SPMB) on glass slides. (A) Schematic illustration of our approach. GPMVs were vesiculated from HEK293T cells, downsized, and placed on a slide. Some vesicles ruptured following adsorption. Addition of synthetic liposomes facilitated the creation of uniform bilayers. (B) Overlay of bright field and confocal fluorescence images of GPMV vesiculation from HEK293T cell stained with DiI dye. (C) Fluorescence microscopy image of GPMVs labeled with DiI dye deposited on a glass surface. (D) Fluorescence microscopy image of downsized GPMVs deposited on a glass surface. (E) Formation of uniform bilayers through the addition of liposomes to the downsized GPMVs, imaged 10 min after liposome addition. A faint dark line was carved on the silica surface intentionally for reference. (F) NTA particle size and concentration analysis of the GPMVs before (black) and after downsizing (red). (G) Normalized FRAP data showing prebleach (red) and postbleach (blue) fluorescence recovery and fitting based on the Soumpasis method for obtaining a diffusion coefficient. (H) Confocal images showing fluorescence recovery after photobleaching of a DiI labeled SPMB. The scale bar is 10 μm. (I) AFM QI mode image of downsized GPMVs showing intact as well as ruptured vesicles. (J) AFM QI mode image of downsized vesicles in the presence of synthetic liposomes showing a continuous bilayer. (K) Height profile corresponding to the line drawn in panel I, showing a membrane bilayer patch and an intact flattened vesicle. (L) Height profile corresponding to the line drawn in panel J showing a bilayer of 4−5 nm thickness.

was carried out on at least 3 different sets of samples, and more than 10 scans were performed for each sample. Nine different areas from 3 different FRAP experiments were analyzed, and the mean values along with the SD are reported. For quantifying the average fluorescence intensity of the microspheres under different conditions; >80 microspheres for each condition were measured, and average values with SD are presented. For Spike-ACE2 interaction studies, the values reported are from at least three independent sets of experiments, as detailed in the caption. Median rupture forces and their standard deviations as reported in the text were determined by bootstrapping with 1000 iterations, resampling 90% of the data. Cumulative distribution functions (CDFs), and bar and box plots were plotted using Origin 9.0 software.

RESULTS

Formation of Supported Plasma Membranes on Planar Glass Surfaces. Prior to coating microspheres, we used glass slides as support for optimizing vesicle concentration to achieve effective vesicle rupture and SPMB

formation (Figure 1A). GPMVs were produced from HEK293T cells labeled with a lipophilic dye, DiI (Figure 1B) (see Methods). The cell-derived GPMVs and other extracellular vesicles in the supernatant varied in size from ~100 nm to 20 μm. When the GPMVs were directly placed on a glass surface, they remained intact or became deflated, maintaining a circular shape (Figure 1C, Table S1). Since we aimed to coat microspheres, we decided to use downsized GPMVs, which allowed us to obtain a high concentration of small vesicles (Figure 1D). When the downsized GPMVs were placed on a glass slide and incubated for 30 min, some of them were ruptured and formed a "grainy" bilayer (Figure 1D, Table S1). The rupture likely occurred via a "parachute-type" mechanism described previously for vesicles,[43,44] where membrane proteins retain their orientation with outward-facing membrane proteins exposed outside of the bilayer. To obtain a continuous membrane bilayer from the downsized vesicles, we followed the method developed by the Daniel
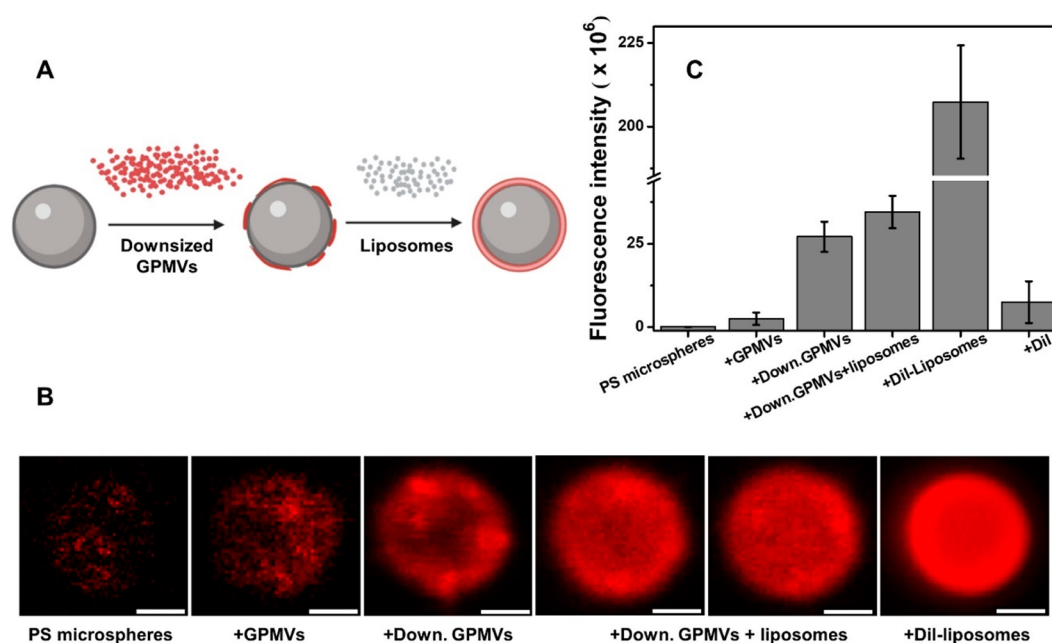
Figure 2. Coating of DiI-GPMVs on polystyrene (PS) microspheres. (A) Illustration of the bead coating procedure. (B) Confocal images of PS microspheres under different coating conditions. Images were taken using LUMICKS confocal fluorescence optical tweezers setup at 60× magnification under the same buffer conditions and same x, y, and z coordinates. Coating conditions are indicated in the labels; label Down.GPMVs corresponds to downsized GPMVs. Scale bars correspond to 1 μm. (C) Average fluorescence intensities of PS microspheres excited at 561 nm under different coating conditions.

group at Cornell University,[18,21] where supported bilayers are formed by adding synthetic liposomes to the preadsorbed natural vesicles, resulting in their rupture. (Figure 1E, Table S1). The lipid composition of the synthetic vesicles was chosen to enhance vesicle rupture.[18,21,45] We found that a ratio of 1:50 of downsized GPMVs to synthetic vesicles formed a continuous SPMB. To quantify the efficiency of GPMV downsizing, we carried out size and concentration measurements using dynamic light scattering (DLS) and nanoparticle tracking analysis (NTA). From the DLS measurements, we observed that the GPMV sample (before downsizing) contained a substantial population of larger vesicles (>1 μm) along with smaller vesicles (~50−120 nm). The population of larger vesicles was completely removed after downsizing, along with an increase in the smaller vesicles' population (~100 nm; Figure S1). To quantify the increase in the concentration of smaller vesicles, we carried out NTA measurements. Before downsizing, the GPMV sample had an average concentration of 1.71×10^9 vesicles/mL with sizes between 30 and 800 nm (we could not quantify the larger vesicles as NTA has a detection limit of ~1 μm at these conditions), whereas after downsizing, the concentration increased to 3.62×10^{10} vesicles/mL, a (~20 ± 4)-fold increase, along with a more uniform size distribution (~110 nm; Figure 1F). HEK293T cells cultured on a 25 cm^2 plate at 80% confluency, yielded a concentration of 8×10^9 to 3×10^{10} downsized vesicles/mL with an average concentration of 1.5×10^{10} vesicles/mL ($n = 5$).

To confirm the formation of continuous SPMB from DiI-GPMVs, we performed fluorescence recovery after photobleaching (FRAP) experiments, where the mobility of DiI-C12 lipids in the bilayer was assessed. We observed significant fluorescence recovery (Figure 1G) and obtained a mobile fraction (M) of 73 ± 2%. We obtained a diffusion coefficient of

0.538 ± 0.27 μm^2/s for the DiI-SPMB, consistent with the reported literature values[25] (Figure 1G,H). Differences from literature values might arise from differences in membrane composition. For reference, we carried out FRAP measurements on membrane bilayers formed from synthetic liposomes containing Rh−PE (Figure S2). Synthetic SMBs showed a mobile fraction of 100 ± 5% with a diffusion coefficient of 1.1 ± 0.28 μm^2/s.

To further confirm the formation of continuous SPMB from GPMVs, we imaged the surfaces with AFM. Deposition of downsized vesicles resulted in multiple intact vesicles ranging from 90 to 420 nm ($n > 40$ vesicles) alongside membrane patches with a thickness of ~5−6 nm, corresponding to bilayers formed from spontaneously ruptured vesicles (Figure 1I). Height profiles of a vesicle and a membrane patch are depicted in Figure 1K. Addition of synthetic liposomes to the supported natural vesicles induced rupture of previously unruptured vesicles (Figure 1J), resulting in a continuous SPMB with an average thickness of 4−5 nm (Figure 1L; a hole is imaged intentionally to demonstrate the layer thickness).

Coating Microspheres with Plasma Membranes. To coat microspheres, we used the optimal ratio of downsized GPMVs to liposomes that was found by using flat surfaces as described above (Figure 2A). Confocal fluorescence images of microspheres coated with GPMVs before and after downsizing with and without added synthetic liposomes are presented in Figure 2B. The images clearly demonstrate that the addition of downsized GPMVs increased the fluorescence coverage on the microsphere compared to regular, large GPMVs, indicating better membrane coverage of the microsphere surface. The addition of synthetic liposomes enhanced vesicle rupture and created a more uniform coating (Figure 2B). We quantified the fluorescence intensity of coated microspheres under different conditions (Figures 2C and S3). Coating microspheres with
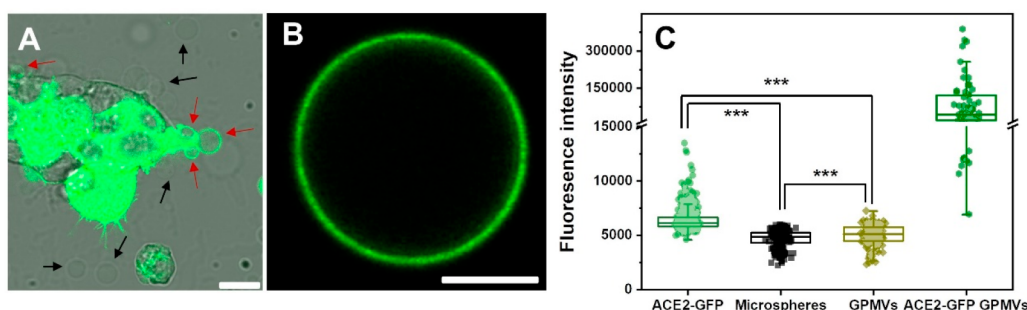
E

Figure 3. (A) Confocal and bright field image overlay of ACE2-GFP transfected HEK293T cells producing GPMVs. Scale bar is 15 μm. The ACE2-GFP GPMVs can be clearly observed (red arrows), along with GPMVs with no fluorescence (black arrows). (B) Confocal image of an isolated GPMV containing ACE2-GFP. Scale bar is 5 μm. (C) Plot showing the fluorescence intensities (number of photons per sphere) of microspheres and GPMVs excited at 488 nm under different conditions. ACE2-GFP = microspheres coated with downsized GPMVs containing ACE2-GFP, $n = 573$. Microspheres = uncoated microspheres, $n = 176$. GPMV = microspheres coated with downsized unlabeled GPMVs, $n = 236$. ACE2-GFP GPMVs = GPMVs containing ACE2-GFP, $n = 63$. The Kolmogorov−Smirnov nonparametric test for all the data showed different distributions of the fluorescence intensity values with *** being $p < 0.001$.
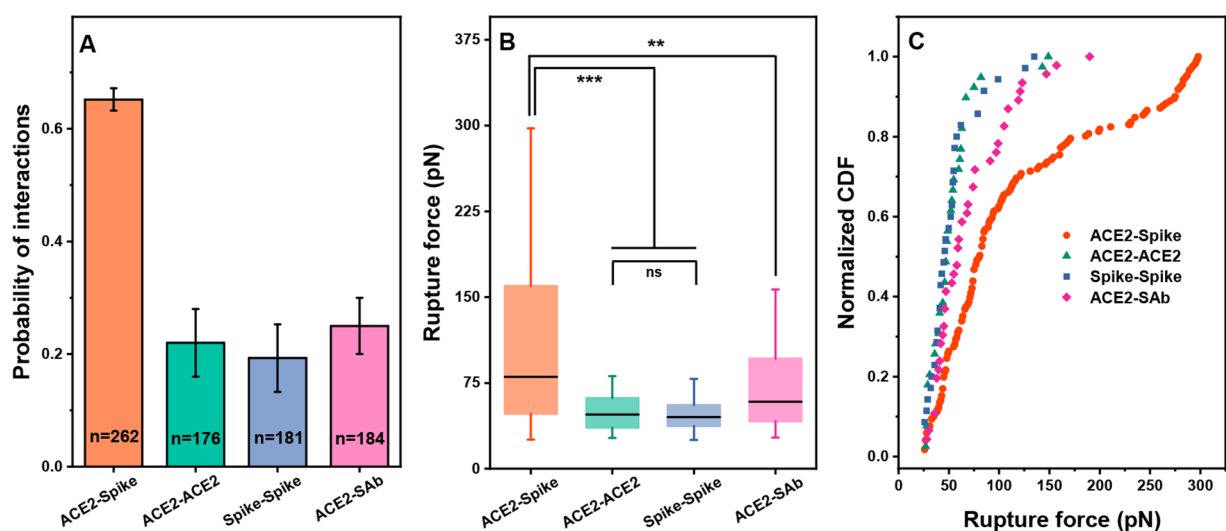

Figure 4. ACE2−Spike interactions measured by force spectroscopy with optical tweezers using microspheres coated with protein-containing natural membranes. (A) Probability of interactions between membranes containing ACE2-coated microspheres and membranes containing Spike-coated microspheres. ACE2-Spike indicates the interaction between ACE2-coated microsphere and Spike-coated microsphere (orange) (pairs = 42, 4 independent experiments). ACE2-ACE2 indicates the interaction between two ACE2-coated microspheres (green) (pairs = 16). Spike−Spike indicates the interaction between two Spike-coated microspheres (blue) (pairs = 21). ACE2-SAb indicates the interaction between ACE2-coated microspheres and Spike-coated microspheres incubated with anti-RBD of Spike antibody (magenta) (pairs = 19). The numbers of approach and separation cycles (n) are indicated for each group. At least 15 microsphere pairs were measured for each sample, with a maximum of 10 cycles for each pair. Error bars indicate the statistical error. (B) Box plot showing the median rupture forces corresponding to the various combinations of ACE2- and Spike-containing microspheres described in panel A. The Kolmogorov−Simrnov non-parametric test for all of the data shows different distributions with *** being $p < 0.001$, ** being $p < 0.01$, and p-ns = 0.73. Box-whisker plot horizontal lines represent (from the top) the maximum, the third quartile, the median, the first quartile, and the minimum. (C) Normalized cumulative distribution functions (CDFs) of the rupture forces.

regular GPMVs was not effective. When we coated the microspheres with downsized vesicles, however, a >10-fold increase in the fluorescence intensity was observed compared to microspheres coated with GPMVs. Several high-fluorescence intensity areas were observed after deposition of downsized GPMVs, which may correspond to membrane patches from spontaneous rupturing of vesicles upon deposition, as observed in the AFM measurements (Figure 1I). To enhance vesicle rupture, in addition to adding synthetic vesicles, we employed gentle heating to 37 °C or introduced the surface-attached layer to an air−water interface[23] (Figure S3).

To further confirm the formation of SPMB on the microspheres, we performed FRAP measurements. Our results clearly demonstrate that continuous and fluid bilayers are formed (Figure S4).

Incorporation of Proteins of Interest in Membranes on Microspheres. In order to validate that the membrane coating contains functional proteins, we decided to measure interactions between two proteins of interest: the Spike of the SARS-CoV-2 and its human receptor, ACE2, as this interaction leads to the entry of SARS-CoV-2 into target cells during infection.[46,47] We produced GPMVs with ACE2−GFP (Figure 3A,B; see Methods for details). It is important to note that GPMVs are heterogeneous in their composition, and not all

GPMVs are fluorescent (Figure 3A). Under our experimental conditions, only ~8% of the GPMVs contained ACE2−GFP (n > 1200 GPMVs; Figure 3B). We next quantified the fluorescence intensity of the coated beads and found ~40% increase in the average fluorescence intensity of the ACE2−GFP microspheres compared to the autofluorescence of the microspheres alone (Figure 3C and Figure S5), indicating that the membranes on the beads contained labeled proteins.

Further, we quantified the ACE2-GFP concentration in the GPMVs as well as on the coated microspheres using soluble GFP and Oregon green as reference fluorophores (see Methods and Figure S6). We determined that the mole fraction of ACE2−GFP in GPMVs varied from 1.5×10^{-4} to 8.5×10^{-3} with an average of $2 \times 10^{-3} \pm 2 \times 10^{-3}$ (n = 55). The mole fraction of ACE2-GFP on the microspheres coated with downsized GPMVs containing ACE2-GFP and fusogenic liposomes in 1:50 ratio was found to vary from 0.85×10^{-4} to 7.5×10^{-4} with an average of $(1.3 \pm 0.7) \times 10^{-4}$ (n = 284).

Optical Tweezers Force Spectroscopy with Membrane Coated Microspheres. In order to examine the functionality of the proteins embedded in the coated membrane, we chose to measure the interactions between the Spike protein of SARS-CoV-2 with its human receptor ACE2. For proper functionality, the proteins need to maintain their correct orientation. First, we validated the activity and competency of the ACE2 and Spike proteins used in this study; we carried out a syncytium assay, where we transiently transfected Spike plasmid in HEK293T cells and transiently co-transfected GFP and ACE2−GFP plasmids in another plate of HEK293T cells, mixed them together, and incubated them with and without the addition of trypsin (Figure S7A). Addition of serine protease enzymes, like trypsin, cleaves the Spike protein,[48] exposing the fusion peptide and leading to cell−cell fusion (Figure S7B). In the presence of trypsin, >50 syncytia were observed per plate, whereas only 3−4 syncytia per plate were observed in the absence of trypsin (Figure S7C). This clearly demonstrates the functionality of the ACE2 and Spike proteins used in our study.

Next, we set out to perform force spectroscopy measurements. The presence of ACE2−GFP in the GPMVs can be observed from GFP fluorescence (Figure 3B), and the presence of SARS-CoV-2 Spike has already been demonstrated in GPMVs.[39] GPMVs were collected and downsized as described above and used to produce SPMB on microspheres; one set of microspheres with ACE2−GFP and another with Spike. To differentiate the two sets of microspheres during our experiments, the Spike transfected cells were stained with DiI (Figure S8). The two types of microspheres were caught in two optical traps and brought into contact with each other by an approach and separation routine in order to measure the unbinding forces, as described previously[26,35] (Figure S9). We observed a high probability of interactions between ACE2−Spike (~65%) compared to the nonspecific interactions between ACE2−ACE2 (21%) and Spike−Spike (19%), indicating the specificity of the ACE2−Spike interaction (Figure 4A). The unbinding forces significantly differed between the specific and nonspecific interactions (Figure 4B). The median rupture force for ACE2−Spike interaction was 81 ± 4.6 pN, whereas ACE2−ACE2 and Spike−Spike had median rupture forces of 47 ± 3.1 and 45 ± 4 pN, respectively (indicated errors are median rupture force standard deviations obtained by bootstrapping with 1000 iterations, resampling 90% of the data of Figure 4C). ACE2−ACE2 and Spike−Spike

unbinding forces are significantly lower than ACE2−Spike, as validated by a two-sample Kolmogorov−Smirnov nonparametric test (p < 0.005). However, ACE2−ACE2 and Spike−Spike interactions exhibit similar distributions (p ns, 0.73).

Next, we performed an antibody-blocking assay[47] to further confirm the specificity of the observed ACE2−Spike binding. Since the ACE2−Spike interaction is mediated by the receptor binding domain (RBD) of Spike, we expected that binding of an RBD-specific antibody to the Spike would inhibit the ACE2−Spike interaction.[49] Microspheres with SPMB containing Spike were incubated with a monoclonal antibody (Ab) specific to Spike RBD (see Methods for details). We observed that Ab-bound Spike showed lower probability of interactions with ACE2 (26%) compared to ACE2−Spike (65%). Comparison of rupture forces with and without added antibody exhibited marked differences (Figures 4B,C). ACE2−SAb unbinding forces were similar to those of ACE2−ACE2 and Spike−Spike, with median values of 59 ± 6.8 pN for ACE2−SAb, 47pN for ACE2−ACE2, 45 pN for Spike−Spike, and 81pN for ACE2−Spike (Figure 4C). These results indicate that anti-RBD Ab was able to bind to the RBD domain of Spike and inhibit ACE2−Spike interactions, further validating the broad applicability of our assay.

■ DISCUSSION

GPMVs are a reliable and facile method of obtaining natural membranes.[15,37] Unlike exosomes, released from intracellular compartments,[17] GPMVs are derived directly from the plasma membrane.[15] GPMVs thus contain plasma membrane constituents in their native conformation, retaining their activity and orientation.[21,22] Expression of transmembrane proteins prior to GPMV production allows preparation of natural membranes with embedded proteins of interest. Here, we present a new method for coating microspheres with natural membranes that are readily compatible with optical trapping. Our method extends the applicability of optical tweezers for unraveling protein−protein interactions in a natural membrane environment while bypassing the need for protein reconstitution. Planar-supported bilayers from natural sources have been previously described.[12,14,18,20−22] However, some applications necessitate the use of spherical microparticles rather than planar surfaces. Studies have been performed with nanoparticles coated with natural membranes from erythrocytes, platelets, macrophages, and cancer cells for various biomedical applications, such as in vivo imaging, photoactivable therapy, and tumor-targeted therapies.[50−53] The common procedure used in these studies is to rupture the cells using a hypotonic solution followed by sonication and coextrusion of the membrane with nanoparticles to facilitate coating. Our method of obtaining natural membranes through GPMVs uses mild conditions and allows us to obtain specific, active membrane proteins of interest embedded within membranes. Our approach could be used to prepare membrane-coated nanoparticles containing membrane proteins of interest for various sensing and biomedical purposes.

We chose to demonstrate the applicability of our method by measuring ACE2−Spike interactions using optical tweezers. To characterize these interactions, we measured unbinding forces and the probability of forming interactions between the Spike of SARS-CoV2 and its receptor, ACE2. We further demonstrated the specificity of the interactions by successfully blocking the binding upon addition of an anti-RBD antibody. These results also demonstrate that our method results in

formation of supported membranes with properly oriented and functional proteins, as this specific interaction could not be possible otherwise. This is in line with previous studies that showed that forming supported natural bilayers from ruptured natural vesicles preserves the correct protein orientation.[43]

Since other reports have demonstrated the potential clinical significance of blocking the ACE2−Spike interactions using an antibody,[46,49] our method could potentially be used as a screening platform to quantitatively assess the blocking efficiency. Previous single molecule studies of the interaction of SARS-CoV2 with ACE2 performed using AFM and magnetic tweezers reported an unbinding force of several tens of piconewtons for the RBD−ACE2 interaction.[54,55] Thus, our measurements likely correspond to several simultaneous unbinding events from multiple (1 to 6) Spike−ACE2 interactions. These studies were conducted using soluble fragments of the proteins in a nonmembranous environment, which could affect protein binding strength in light of a recent study that showed that the infectivity of SARS-CoV2 in the presence of membrane-bound ACE2 is much higher compared to that of soluble ACE2,[56] emphasizing the importance of studying such protein−protein interactions within membranes.

CONCLUSION

We developed a new tool for protein−protein interaction studies, based on natural membranes obtained from giant plasma membrane vesicles, which allows working with membrane proteins of interest within a background of native membrane components while avoiding the need for reconstitution. We expect our approach to be broadly adopted and used in studies of various membrane biology and biophysics questions.

ASSOCIATED CONTENT

Ⓢ Supporting Information

The Supporting Information is available free of charge at https://pubs.acs.org/doi/10.1021/acsami.2c13095.

DLS profile; normalized FRAP data; confocal images; average fluorescence intensities; FRAP typical examples; fluorescence intensities; syncytium assays; schematic, bright field, and fluorescence images; force−distance plots; fluorescence intensity data (PDF)

AUTHOR INFORMATION

Corresponding Author

Raya Sorkin − Raymond and Beverly Sackler Faculty of Exact Sciences, School of Chemistry, Tel Aviv University, Tel Aviv, Israel 6997801; Center for Physics and Chemistry of Living Systems and Center for Light-Matter Interaction, Tel Aviv University, Tel Aviv, Israel 6997801; ⓞ orcid.org/0000-0001-9006-5411; Email: rsorkin@tauex.tau.ac.il

Authors

Sudheer K. Cheppali − Raymond and Beverly Sackler Faculty of Exact Sciences, School of Chemistry, Tel Aviv University, Tel Aviv, Israel 6997801; Center for Physics and Chemistry of Living Systems and Center for Light-Matter Interaction, Tel Aviv University, Tel Aviv, Israel 6997801

Raviv Dharan − Raymond and Beverly Sackler Faculty of Exact Sciences, School of Chemistry, Tel Aviv University, Tel Aviv, Israel 6997801; Center for Physics and Chemistry of

Living Systems and Center for Light-Matter Interaction, Tel Aviv University, Tel Aviv, Israel 6997801

Roni Katzenelson − Raymond and Beverly Sackler Faculty of Exact Sciences, School of Chemistry, Tel Aviv University, Tel Aviv, Israel 6997801; Center for Physics and Chemistry of Living Systems and Center for Light-Matter Interaction, Tel Aviv University, Tel Aviv, Israel 6997801

Complete contact information is available at:
https://pubs.acs.org/10.1021/acsami.2c13095

■ REFERENCES

(1) Simons, K.; Sampaio, J. Membrane Organization and Lipid Rafts. Cold Spring Harbor Perspect. Biol. 2011, 3, a004697.

(2) Dupuy, A. D.; Engelman, D. M. Protein Area Occupancy at the Center of the Red Blood Cell Membrane. Proc. Natl. Acad. Sci. U. S. A. 2008, 105 (8), 2848−2852.

(3) Fung, T. S.; Liu, D. X. Human Coronavirus : Host-Pathogen Interaction. Annaul Rev. Microbiol. 2019, 73, 529−560.

(4) Cheng, X.; Smith, J. C. Biological Membrane Organization and Cellular Signaling. Chem. Rev. 2019, 119, 5849−5880.

(5) Schlessinger, J. Cell Signaling by Receptor Tyrosine Kinases A Large Group of Genes in All Eukaryotes Encode For. Cell 2000, 103, 211−225.

(6) Ruta, V.; Jiang, Y.; Lee, A.; Chen, J.; MacKinnon, R. Functional Analysis of an Archaebacterial Voltage-Dependent K+ Channel. Nature 2003, 422 (6928), 180−185.

(7) Witkowska, A.; Jahn, R. Rapid SNARE-Mediated Fusion of Liposomes and Chromaffin Granules with Giant Unilamellar Vesicles. Biophys. J. 2017, 113 (6), 1251−1259.

(8) Witkowska, A.; Jablonski, L.; Jahn, R. A Convenient Protocol for Generating Giant Unilamellar Vesicles Containing SNARE Proteins Using Electroformation. Sci. Rep. 2018, 8 (1), 9422.

(9) Aimon, S.; Manzi, J.; Schmidt, D.; Poveda Larrosa, J. A.; Bassereau, P.; Toombes, G. E. S. Functional Reconstitution of a Voltage-Gated Potassium Channel in Giant Unilamellar Vesicles. PLoS One 2011, 6 (10), e25529.

(10) Verchere, A.; Broutin, I.; Picard, M.Reconstitution of Membrane Proteins in Liposomes. In Membrane Protein Structure and Function Characterization; Methods in Molecular Biology, Vol. 1635; Humana Press, 2017; pp 259−282. DOI: 10.1007/978-1-4939-7151-0_14.

(11) Dimova, R.; Marques, C.The Giant Vesicle Book; CRC Press, 2019.

(12) Richards, M. J.; Hsia, C.; Singh, R. R.; Haider, H.; Kumpf, J.; Kawate, T.; Daniel, S. Membrane Protein Mobility and Orientation Preserved in Supported Bilayers Created Directly from Cell Plasma Membrane Blebs. Langmuir 2016, 32, 2963−2974.

(13) Costello, D. A.; Millet, J. K.; Hsia, C. Y.; Whittaker, G. R.; Daniel, S. Single Particle Assay of Coronavirus Membrane Fusion with Proteinaceous Receptor-Embedded Supported Bilayers. Biomaterials 2013, 34 (32), 7895−7904.

(14) Uribe, J.; Liu, H.; Mohamed, Z.; Chiou, A. E.; Fischbach, C.; Daniel, S. Supported Membrane Platform to Assess Surface Interactions between Extracellular Vesicles and Stromal Cells. *ACS Biomater. Sci. 7 Eng.* **2020**, *6*, 3945−3956.

(15) Sezgin, E.; Kaiser, H. J.; Baumgart, T.; Schwille, P.; Simons, K.; Levental, I. Elucidating Membrane Structure and Protein Behavior Using Giant Plasma Membrane Vesicles. *Nat. Protoc.* **2012**, *7* (6), 1042−1051.

(16) Scott, R. E. Plasma Membrane Vesiculation: A New Technique for Isolation of Plasma Membranes. *Science (80-.)* **1976**, *194* (4266), 743−745.

(17) Cocucci, E.; Meldolesi, J. Ectosomes and Exosomes: Shedding the Confusion between Extracellular Vesicles. *Trends Cell Biol.* **2015**, *25* (6), 364−372.

(18) Costello, D. A.; Hsia, C. Y.; Millet, J. K.; Porri, T.; Daniel, S. Membrane Fusion-Competent Virus-like Proteoliposomes and Proteinaceous Supported Bilayers Made Directly from Cell Plasma Membranes. *Langmuir* **2013**, *29* (21), 6409−6419.

(19) Peerboom, N.; Schmidt, E.; Trybala, E.; Block, S.; Bergström, T.; Pace, H. P.; Bally, M. Cell Membrane Derived Platform to Study Virus Binding Kinetics and Diffusion with Single Particle Sensitivity. *ACS Infect. Dis.* **2018**, *4* (6), 944−953.

(20) Liu, H. Y.; Grant, H.; Hsu, H. L.; Sorkin, R.; Bošković, F.; Wuite, G.; Daniel, S. Supported Planar Mammalian Membranes as Models of in Vivo Cell Surface Architectures. *ACS Appl. Mater. Interfaces* **2017**, *9* (41), 35526−35538.

(21) Su, H.; Liu, H. Y.; Pappa, A. M.; Hidalgo, T. C.; Cavassin, P.; Inal, S.; Owens, R. M.; Daniel, S. Facile Generation of Biomimetic-Supported Lipid Bilayers on Conducting Polymer Surfaces for Membrane Biosensing. *ACS Appl. Mater. Interfaces* **2019**, *11* (47), 43799−43810.

(22) Pappa, A. M.; Liu, H. Y.; Walther, T.-C.; Thiburse, Q.; Savva, A.; Pamia, A.; Salleo, A.; Daniel, S.; Owens, R. M. Optical and Electronic Ion Channel Monitoring from Native Human Membranes. *ACS Nano* **2020**, *14* (10), 12538−12545.

(23) Chiang, P. C.; Tanady, K.; Huang, L. T.; Chao, L. Rupturing Giant Plasma Membrane Vesicles to Form Micron-Sized Supported Cell Plasma Membranes with Native Transmembrane Proteins. *Sci. Rep.* **2017**, *7* (1), 15139.

(24) Sezgin, E.; Carugo, D.; Levental, I.; Stride, E.; Eggeling, C. Creating Supported Plasma Membrane Bilayers Using Acoustic Pressure. *Membranes (Basel).* **2020**, *10* (2), 30.

(25) Teiwes, N. K.; Mey, I.; Baumann, P. C.; Strieker, L.; Unkelbach, U.; Steinem, C. Pore-Spanning Plasma Membranes Derived from Giant Plasma Membrane Vesicles. *ACS Appl. Mater. Interfaces* **2021**, *13* (22), 25805−25812.

(26) Sorkin, R.; Marchetti, M.; Logtenberg, E.; Piontek, M. C.; Kerklingh, E.; Brand, G.; Voleti, R.; Rizo, J.; Roos, W. H.; Groffen, A. J.; Wuite, G. J. L. Synaptotagmin-1 and Doc2b Exhibit Distinct Membrane-Remodeling Mechanisms. *Biophys. J.* **2020**, *118* (3), 643−656.

(27) Ma, L.; Cai, Y.; Li, Y.; Jiao, J.; Wu, Z.; O'Shaughnessy, B.; De Camilli, P.; Karatekin, E.; Zhang, Y. Single-Molecule Force Spectroscopy of Protein-Membrane Interactions. *eLife* **2017**, *6*, e30493.

(28) Ge, J.; Bian, X.; Ma, L.; Cai, Y.; Li, Y.; Yang, J.; Karatekin, E.; De Camilli, P.; Zhang, Y. Stepwise Membrane Binding of Extended Synaptotagmins Revealed by Optical Tweezers. *Nat. Chem. Biol.* **2022**, *18*, 313−320.

(29) Dame, R. T.; Noom, M. C.; Wuite, G. J. L. Bacterial Chromatin Organization by H-NS Protein Unravelled Using Dual DNA Manipulation. *Nature* **2006**, *444* (7117), 387−390.

(30) Qu, E.; Guo, H.; Xu, C.; Liu, C.; Li, Z.; Cheng, B.; Zhang, D. Method Used to Measure Interaction of Proteins with Dual-Beam Optical Tweezers. *J. Biomed. Opt.* **2006**, *11*, 064035.

(31) Stout, A. L. Detection and Characterization of Individual Intermolecular Bonds Using Optical Tweezers. *Biophys. J.* **2001**, *80* (6), 2976−2986.

(32) Zhou, Z. L.; Tang, B.; Ngan, A. H. W.; Dong, Z. N.; Wu, Y. S. Hepatitis B Surface Antigen-Antibody Studied by Optical Tweezers. *IET Nanobiotechnology* **2012**, *6* (1), 9−15.

(33) Cheppali, S. K.; Dharan, R.; Sorkin, R. Forces of Change : Optical Tweezers in Membrane Remodeling Studies. *J. Membr. Biol.* **2022**, DOI: 10.1007/s00232-022-00241-1.

(34) Dols-Perez, A.; Marin, V.; Amador, G. J.; Kieffer, R.; Tam, D.; Aubin-Tam, M. E. Artificial Cell Membranes Interfaced with Optical Tweezers: A Versatile Microfluidics Platform for Nanomanipulation and Mechanical Characterization. *ACS Appl. Mater. Interfaces* **2019**, *11* (37), 33620−33627.

(35) Brouwer, I.; Giniatullina, A.; Laurens, N.; Van Weering, J. R. T.; Bald, D.; Wuite, G. J. L.; Groffen, A. J. Direct Quantitative Detection of Doc2b-Induced Hemifusion in Optically Trapped Membranes. *Nat. Commun.* **2015**, *6*, 1−8.

(36) Murray, D. H.; Jahnel, M.; Lauer, J.; Avellaneda, M. J.; Brouilly, N.; Cezanne, A.; Morales-Navarrete, H.; Perini, E. D.; Ferguson, C.; Lupas, A. N.; Kalaidzidis, Y.; Parton, R. G.; Grill, S. W.; Zerial, M. An Endosomal Tether Undergoes an Entropic Collapse to Bring Vesicles Together. *Nature* **2016**, *537* (7618), 107−111.

(37) Gerstle, Z.; Desai, R.; Veatch, S. L. Giant Plasma Membrane Vesicles: An Experimental Tool for Probing the Effects of Drugs and Other Conditions on Membrane Domain Stability. *Methods Enzymol.* **2018**, *603*, 129−150.

(38) Sezgin, E. Giant Plasma Membrane Vesicles to Study Plasma Membrane Structure and Dynamics. *Biochim. Biophys. Acta - Biomembr.* **2022**, *1864* (4), 183857.

(39) Sanders, D. W.; Jumper, C. C.; Ackerman, P. J.; Bracha, D.; Donlic, A.; Kim, H.; Kenney, D.; Castello-serrano, I.; Suzuki, S.; Tamura, T.; Tavares, A. H.; Saeed, M.; Holehouse, A. S.; Ploss, A.; Levental, I.; Douam, F.; Padera, R. F.; Levy, B. D.; Brangwynne, C. P. SARS-CoV-2 Requires Cholesterol for Viral Entry and Pathological Syncytia Formation. *Elife* **2021**, *10*, e65962.

(40) Soumpasis, D. M. Theoretical Analysis of Fluorescence Photobleaching Recovery Experiments. *Biophys. J.* **1983**, *41*, 95−97.

(41) Steinkühler, J.; Knorr, R. L.; Zhao, Z.; Bhatia, T.; Bartelt, S. M.; Wegner, S.; Dimova, R.; Lipowsky, R. Controlled division of cell-sized vesicles by low densities of membrane-bound proteins. *Nat. Commun.* **2020**, *11*, 905.

(42) Dharan, R.; Goren, S.; Cheppali, S. K.; Shendrik, P.; Brand, G.; Yu, L.; Kozlov, M. M.; Sorkin, R. Transmembrane Protein Tetraspinin 4 and CD9 Sense Membrane Curvature. *PNAS* **2022**, *119* (43), e2208993119. DOI: 10.1073/pnas.2208993119.

(43) Richards, M. J.; Hsia, C.; Singh, R. R.; Haider, H.; Kumpf, J.; Kawate, T.; Daniel, S. Membrane Protein Mobility and Orientation Preserved in Supported Bilayers Created Directly from Cell Plasma Membrane Blebs. *Langmuir* **2016**, *32*, 2963−2974.

(44) Fuhrmans, M.; Muller, M. Mechanisms of Vesicle Spreading on Surfaces: Coarse-Grained Simulations. *Langmuir* **2013**, *29*, 4335−4340.

(45) Schmid, Y. R. F.; Scheller, L.; Buchmann, S.; Dittrich, P. S. Calcium-Mediated Liposome Fusion to Engineer Giant Lipid Vesicles with Cytosolic Proteins and Reconstituted Mammalian Proteins. *Adv. Biosys.* **2020**, *4*, 2000153.

(46) Taylor, P. C.; Adams, A. C.; Hufford, M. M.; de la Torre, I.; Winthrop, K.; Gottlieb, R. L. Neutralizing Monoclonal Antibodies for Treatment of COVID-19. *Nat. Rev. Immunol.* **2021**, *21*, 382−393.

(47) Ou, X.; Liu, Y.; Lei, X.; Li, P.; Mi, D.; Ren, L.; Guo, L.; Guo, R.; Chen, T.; Hu, J.; Xiang, Z.; Mu, Z.; Chen, X.; Chen, J.; Hu, K.; Jin, Q.; Wang, J.; Qian, Z. Characterization of Spike Glycoprotein of SARS-CoV-2 on Virus Entry and Its Immune Cross-Reactivity with SARS-CoV. *Nat. Commun.* **2020**, *11*, 1620.

(48) Tang, T.; Bidon, M.; Jaimes, J. A.; Whittaker, G. R.; Daniel, S. Coronavirus Membrane Fusion Mechanism Offers a Potential Target for Antiviral Development. *Antiviral Res.* **2020**, *178* (March), 104792.

(49) Ejemel, M.; Li, Q.; Hou, S.; Schiller, Z. A.; Tree, J. A.; Wallace, A.; Amcheslavsky, A.; Kurt Yilmaz, N.; Buttigieg, K. R.; Elmore, M. J.; Godwin, K.; Coombes, N.; Toomey, J. R.; Schneider, R.; Ramchetty, A. S.; Close, B. J.; Chen, D.-Y.; Conway, H. L.; Saeed, M.; Ganesa, C.;

Carroll, M. W.; Cavacini, L. A.; Klempner, M. S.; Schiffer, C. A.; Wang, Y. A Cross-Reactive Human IgA Monoclonal Antibody Blocks SARS-CoV-2 Spike-ACE2 Interaction. *Nat. Commun.* **2020**, *11*, 4198.

(50) Gao, W.; Hu, C.-M. J.; Fang, R. H.; Luk, B. T.; Su, J.; Zhang, L. Surface Functionalization of Gold Nanoparticles with Red Blood Cell Membranes. *Adv. Mater.* **2013**, *25*, 3549−3553.

(51) Fang, R. H.; Kroll, A. V.; Gao, W.; Zhang, L. Cell Membrane Coating Nanotechnology. *Adv. Mater.* **2018**, *30*, 1706759.

(52) Xuan, M.; Shao, J.; Dai, L.; He, Q.; Li, J. Macrophage Cell Membrane Camoufl Aged Mesoporous Silica Nanocapsules for In Vivo Cancer Therapy. *Adv. Healthc. Mater.* **2015**, *4*, 1645−1652.

(53) Hu, C. M. J.; Fang, R. H.; Wang, K. C.; Luk, B. T.; Thamphiwatana, S.; Dehaini, D.; Nguyen, P.; Angsantikul, P.; Wen, C. H.; Kroll, A. V.; Carpenter, C.; Ramesh, M.; Qu, V.; Patel, S. H.; Zhu, J.; Shi, W.; Hofman, F. M.; Chen, T. C.; Gao, W.; Zhang, K.; Chien, S.; Zhang, L. Nanoparticle Biointerfacing by Platelet Membrane Cloaking. *Nature* **2015**, *526* (7571), 118−121.

(54) Bauer, M. S.; Gruber, S.; Hausch, A.; Gomes, P. S. F. C.; Milles, L. F.; Nicolaus, T.; Schendel, L. C.; Navajas, P.; Procko, E.; Lietha, D.; Melo, M. C. R.; Bernardi, R. C.; Gaub, H. E.; Lipfert, J. A Tethered Ligand Assay to Probe SARS-CoV-2:ACE2 Interactions. *Proc. Natl. Acad. Sci. U. S. A.* **2022**, *119* (14), 1−11.

(55) Yang, J.; Petitjean, S. J. L.; Koehler, M.; Chen, W.; Derclaye, S.; Vincent, S. P.; Zhang, Q.; Dumitru, A. C.; Soumillion, P.; Alsteens, D. Molecular Interaction and Inhibition of SARS-CoV-2 Binding to the ACE2 Receptor. *Nat. Commun.* **2020**, *11*, 4541.

(56) Batlle, D.; Monteil, V.; Garreta, E.; Hassler, L.; Wysocki, J.; Chandar, V.; Schwartz, R. E.; Mirazimi, A.; Montserrat, N.; Bader, M.; Penninger, J. M. Evidence in Favor of the Essentiality of Human Cell Membrane-Bound ACE2 and against Soluble ACE2 for SARS-CoV-2 Infectivity. *Cell* **2022**, *185* (11), 1837−1839.